buildings

MDPI

Article

Study on Mechanical Properties and Microscopic Mechanisms of Alkali-Activated Coal Gangue Cementitious Materials

Xuejing Zhang [1], Mingyuan Zhou [1], Yuan Mei [2,*] and Hongping Lu [2]

[1] Shaanxi Building Materials Technology Group Co., Ltd., Xi'an 710018, China; zhxj2007raohe@163.com (X.Z.)
[2] School of Civil Engineering, Xi'an University of Architecture and Technology, Xi'an 710055, China
* Correspondence: my0326@126.com

Abstract

Alkali-activated cementitious materials (AACMs) are recognized as promising green building materials and a viable alternative to traditional cement due to their low carbon footprint, high durability, and superior mechanical properties. These materials primarily utilize industrial by-products such as coal gangue, steel slag, and gasification slag. The alkali activation process offers an environmentally friendly pathway for the construction industry. To address the need for the large-scale utilization of bulk solid wastes, this study established a ternary solid waste synergy system comprising coal gangue, steel slag, and gasification slag. The preparation and performance optimization of AACMs based on this system were investigated. An optimal mix proportion was identified through orthogonal experiments, and the influence of various factors on the mechanical properties at different curing ages was analyzed. The results indicate that the fluidity of all AACMs meets the requirements for general backfilling applications. Among the alkali activators, Na_2SO_4 had the smallest effect on fluidity. Under single-activator conditions, sodium silicate (water glass) and sodium hydroxide exerted a greater influence on strength development compared to anhydrous sodium sulfate. For the composite activator system, the significance of parameters affecting compressive strength followed the order: silicate modulus > alkali activator content. The maximum 28-day unconfined compressive strength reached 7.653 MPa with a mix proportion of 55% coal gangue, 45% steel slag, and 5% gasification slag, as well as a silicate modulus of 1.2 and a water glass content of 8%. This represents increases of 540.95% and 299.25% compared to the non-activated group and single-activator groups, respectively. Microstructural analysis revealed that the enhanced integrity and strength of AACMs are attributed to pore-filling by hydration products, predominantly C–S–H and C–A–S–H gels. This study successfully developed high-performance AACMs based on a coal gangue–steel slag–gasification slag ternary system, elucidating the critical regulatory role of silicate modulus in composite activators and the underlying microstructural strengthening mechanisms. The findings provide a theoretical foundation and technical support for the high-value, large-scale utilization of bulk industrial solid wastes in building materials.

Keywords: industrial solid waste; cementitious material; alkali activation; unconfined compressive strength; microstructure; orthogonal test

Check for updates

Academic Editor: Eugeniusz Koda

Received: 9 December 2025
Revised: 13 March 2026
Accepted: 19 March 2026
Published: 12 April 2026

Copyright: © 2026 by the authors. Licensee MDPI, Basel, Switzerland. This article is an open access article distributed under the terms and conditions of the Creative Commons Attribution (CC BY) license.

1. Introduction

Accelerated urbanization has brought about a great deal of demolition and reconstruction, resulting in a large amount of construction waste [1]. Construction waste accounts

for 40% of urban solid waste, and a large amount of construction waste has not been recycled [2]. Every year, there are enormous challenges associated with building and demolition waste, with amounts up to 850, 5, and 15 million tons in the European Union, the United States, and China, respectively [3]. Coal gangue pile is a kind of heterogeneous loose medium composed of gangue particles with different particle sizes and shapes. Because of the low porosity of the upper part, heat accumulation can easily occur. When the temperature is enough to reach the ignition temperature of combustible materials, spontaneous combustion will occur, which will cause serious harm to the environment and society [4]. Coal gangue, as the main solid waste derived from coal mining, has become an urgent environmental problem to be solved due to the encroachment on land resources and the ecological destruction caused by its disorderly storage. At present, there are many ways to use waste coal gangue, such as filling materials, preparation of calcined kaolin, coal gangue-based power generation, as aluminum-based chemical raw materials, preparation of sintered bricks for construction, preparation of cement clinker mixtures, preparation of environmental protection materials and as concrete coarse aggregate [5,6]. Steel slag is recycled as a smelting solvent in our factory to replace limestone and recover a large amount of Fe and other elements such as Mn, Ni and Cu [7–10].

Alkali-activated cementitious material is an inorganic polymer with a three-dimensional network structure formed by a polymerization reaction initiated by an alkaline activator using active SiO_2 and Al_2O_3 aluminum silicate solid waste as raw materials. It has the advantages of low energy consumption, low carbon emissions, low hydration heat and excellent durability. It is a potential cement substitute material [11–15]. The most commonly used alkali-activated raw materials are coal gangue, steel slag, metakaolin and other industrial by-products or natural minerals rich in silicon and aluminum. Although metakaolin exhibits high activity and can be solidified at room temperature, its application is limited due to its high price [16]. Coal gangue and steel slag are the most commonly used alkali-activated materials at present [17]. Under the action of an activator, alkali-activated materials undergo a series of chemical reactions such as dissolution and polymerization, and the molecules are rearranged into an amorphous gel network structure. This is different to ordinary Portland cement. The hydration products of Portland cement are mainly composed of inorganic small molecules with a low degree of polymerization, which is very different from alkali-activated cementitious materials with their high degree of polymerization [18–25]. Palmero et al. [26,27] found that, in a strong alkali environment, after a series of chemical reactions such as the dissolution and polymerization of raw materials, a new type of gel structure forms through molecular recombination and arrangement. According to the different calcium contents (mass ratio of CaO) in raw materials, the formation of gel types is also different. The hydration products of alkali-activated materials with low calcium content are mainly sodium aluminosilicate hydrate (N-A-S-H) gel or potassium aluminosilicate hydrate (K-A-S-H) gel. The hydration products of alkali-activated materials with high calcium content are mainly calcium aluminosilicate hydrate (C-A-S-H) gel or calcium silicate hydrate (C-S-H) gel [28–32].

In recent years, studies have shown that coal gangue has the characteristics of pozzolanic active substances, and can form a hydraulic cementitious system after alkali excitation. As an alternative material to Portland cement, it shows significant application potential in the field of building materials [33–35]. This technology path not only realizes the high-value utilization of bulk solid waste, but also produces considerable carbon emission reduction benefits by reducing the dependence of the cement industry, and synergistically promotes the development of solid waste recycling and low-carbon building materials [36–39]. Research currently focuses on the active excitation mechanism of coal gangue-based materials: Zhang et al. [40] revealed the regulation of the modulus of a

water glass–sodium hydroxide composite activator on the fluidity, compressive strength and microstructure of a geopolymer. Ma [41] discussed the effects of activator modulus, slag content and activator solid content on the compressive strength and drying shrinkage of coal gangue–slag mortar. It was found that a higher slag content and water glass modulus would induce the mortar to experience a longer drying shrinkage period. Han et al. [42] systematically summarized the activation methods of coal gangue, and proposed to optimize the mechanical properties and workability of a coal gangue geopolymer by alkali content, sodium silicate modulus, curing conditions and calcium-based materials. Cheng et al. [43] discussed the chloride binding properties of alumina-rich coal gangue cementitious materials. The phase composition of the samples was analyzed by XRD and TG-DTG. The product of the auxiliary cementitious material containing Al_2O_3 contained Friedel's salt. With the increase in the Ca/Si and Si/Al molar ratios, the chloride binding capacity of the coal gangue samples first increased and then decreased. Using a Box–Benhnken design in the surface response method, Zhou Mei et al. [44] revealed that the 28 d compressive strength is optimal when the content of coal gangue powder is 40%, the modulus of water glass is 1.6, and the content of water glass is 12.2%. Coal gangue powder\fly ash provides mechanical strength by dissolution, monomer reconstruction and polycondensation to form an amorphous phase C- (N)-S-A-H gel. Ma [45] used NaOH and Na_2SiO_3 alkali activators to prepare a coal gangue–slag geopolymer. The results show that the liquid–solid ratio is the main factor affecting the fluidity and strength of alkali-activated coal gangue cementitious materials. In addition, with the increase in the Ca/Si ratio, Ca^{2+} in high-calcium slag promotes the exchange with Na^+, and the product is transformed from a N-A-S-H gel to a C-(A)-S-H gel. Many scholars have shown that a single alkali-activated cementitious material cannot make full use of its various components, but that diversified solid waste has a complementary effect. They together form a calcium–silicon–aluminum precursor combination, and there is a synergistic excitation effect [46–49].

Although significant progress has been made in existing research, the current knowledge system still faces the following unresolved issues: (1) the synergistic alkali-activation effect and mechanism of the specific ternary solid waste combination of coal gangue, steel slag, and gasification slag have not been systematically studied; (2) the key regulatory roles played by the alkali activator modulus and content in compressive strength and microstructural properties in multi-component composite systems remain unclear; (3) most studies focus on the development of compressive strength, while insufficient attention has been paid to mix design methods that synergistically optimize fluidity and strength.

Therefore, to deepen understanding of the synergistic activation mechanisms of multi-source solid wastes and promote their engineering application, this study selects coal gangue, steel slag, and gasification slag to construct a ternary solid waste system. Using sodium silicate, sodium hydroxide, and anhydrous sodium sulfate as activators, we systematically investigate the effects of different activator types, moduli, and dosages on the fluidity and unconfined compressive strength of the cementitious materials. The novelty of this work lies in (1) for the first time, conducting systematic research and mix optimization on the synergistic alkali-activation performance of a "coal gangue–steel slag–gasification slag" ternary system; (2) employing orthogonal experiments combined with efficacy coefficient method to achieve multi-objective synergistic optimization of material fluidity and mechanical properties; (3) elucidating the product evolution and structural strengthening mechanisms of this ternary system under alkali activation through microstructural characterization techniques such as XRD and SEM, thereby clarifying the critical role of alkali modulus. This study aims to provide theoretical foundations and technical support for the high-value resource utilization of industrial solid wastes and the development of low-carbon cementitious materials.

2. Materials and Methods

2.1. Materials

The coal gangue used in this experiment was selected from Huangling No. 1 and Huangling No. 2 mining areas; steel slag was selected from Hancheng Renault powder (Hancheng Leinuo Powder Technology Co., Ltd., Hancheng, China); the gasification slag was selected from the waste slag field of Pucheng Clean Energy Chemical Co., Ltd. (Pucheng, China); and the samples passing through the 5 mm sieve were selected as the basic raw materials for the indoor test. The main chemical components of the raw materials are shown in Table 1, and the grain distribution of the three materials is shown in Figure 1.

Sodium hydroxide (NaOH) is a white crystal flake of analytical purity ($\geq$ 96%); sodium sulfate acid (Na_2SO_4) of chemical purity (concentration $\geq$ 99.0%); and the water glass selected in the experiment is made of water glass stock solution (Na_2SiO_3) and sodium hydroxide, and the modulus of the water glass is adjusted by adding sodium hydroxide. According to the needs of the experimental design, the modulus of the water glass needs to be adjusted to three different moduli: 1.0, 1.2 and 1.4. The specific parameter values of the water glass stock solution are shown in Table 2.

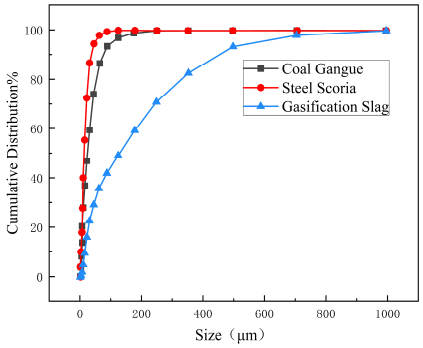


Figure 1. Cumulative particle size distribution of three different materials.

Table 1. Main chemical components of raw materials.

Raw Material	The Main Chemical Composition %						
	SiO_2	Al_2O_3	Fe_2O_3	K_2O	MgO	CaO	Na_2O
Coal Gangue	59.54	23.64	6.12	4.12	2.04	1.85	1.08
Steel Scoria	22.24	10.17	3.46	1.14	1.23	57.84	0.29
Gasification Slag	45.07	18.52	12.27	1.38	4.53	14.11	4.12

Table 2. Parameter values of sodium silicate stock solution.

SiO_2 Content/wt %	Na_2O Content/wt%	Silicate Modulus	Baumé Gravity/°Bé
26.2	8.3	3.2	38

2.2. Mix Proportions

Cementitious materials were prepared using a ternary system of coal gangue, steel slag, and gasification slag under alkali activation. The baseline mix proportion was set as follows: coal gangue 55%, steel slag 40%, gasification slag 5%, and water–binder ratio 0.43. Three alkali activators—sodium silicate (Na_2SiO_3), sodium hydroxide (NaOH), and sodium sulfate (Na_2SO_4)—were used in orthogonal experiments, as detailed in Table 3. Group N0 served as the control without alkali activator. Groups N1–N9 examined the effects on mechanical properties of single activators at varying dosages. Groups W1–W9 investigated the influence on mechanical properties of water glass modulus and alkali content.

Table 3. Mix proportions of alkali-activated cementitious materials.

Specimens	Alkali Activator	Modulus	Activator Content/wt%
N0	—	—	0
N1	NaOH	—	6
N2			8
N3			10
N4	Na_2SO_4		6
N5			8
N6			10
N7	Na_2SiO_3		6
N8			8
N9			10
W1	Water Glass	1.0	6
W2			8
W3			10
W4		1.2	6
W5			8
W6			10
W7		1.4	6
W8			8
W9			10

2.3. Specimen Preparation and Maintenance

The cementitious material specimens were primarily prepared by manual mixing. Flake NaOH or anhydrous Na_2SO_4 solid were dissolved in deionized water at 30–40 °C, stirred until completely dissolved to prepare the required solution, then sealed and left to stand for 24 h to reach room temperature. This ensured solution homogeneity and eliminated the effects of dissolution heat. For the sodium silicate activator, the mass of NaOH solid required to be added to the stock sodium silicate solution was calculated based on the target modulus (1.0, 1.2, 1.4) and dosage. Flake sodium hydroxide was poured into a beaker containing water at 30–40 °C while stirring continuously until completely dissolved. The resulting sodium hydroxide solution was then left to stand for 24 h. Subsequently, this sodium hydroxide solution was poured into the stock sodium silicate solution under constant stirring. After complete mixing, the solution was left to stand for 3 h to obtain the required sodium silicate solution.

Coal gangue, steel slag, gasification slag, and the alkali activator were weighed according to the proportions specified in Table 3. For each mixture proportion, 18 specimens were prepared. The mixtures were placed into triple mortar molds measuring 70.7 mm × 70.7 mm × 70.7 mm, compacted, and cured within the molds for 24 to 48 h. After demolding using a demolding apparatus, the specimens were renumbered. They were then placed in the corresponding curing environments according to their serial numbers and cured further until the designated testing ages.

2.4. Test Method

2.4.1. Fluidity Test

The fluidity test was conducted using a slump cone. During the test, the slump cone was placed on a waterproof cloth. The composite cementitious mixture was filled into the cone in three layers, with the height of each layer after filling approximately one-third of the cone's height. Each layer was rodded spirally from the edge toward the center. After the entire filling process was completed, excess material was struck off and the top surface was leveled with a trowel. The slump cone was then immediately lifted vertically. A steel ruler was used to measure the spread diameter of the mixture in two perpendicular horizontal directions after it had stabilized. The arithmetic mean of the two spread diameters was taken as the fluidity value of the composite cementitious material. The test process is shown in Figure 2.



Figure 2. Liquidity measurement setup.

By referencing relevant domestic and international test methods and evaluation standards, and considering the available laboratory equipment, this study established its own fluidity test method and evaluation criteria. The dimensions of the slump cone were as follows: height 300 mm ± 0.5 mm, top inner diameter 100 mm ± 0.5 mm, and bottom inner diameter 200 mm ± 0.5 mm. The waterproof cloth measured 1500 mm × 1500 mm. The classification criteria for fluidity are presented in Table 4.

Table 4. Fluidity grading standard.

Fluidity/mm	Evaluation Grade	Sphere of Application
<250	Poor	Large space pipe trench, roadbed and other backfill projects
250–350	Medium	General Backfill Engineering
>350	Good	Narrow operation space or dead angle and other backfill projects

2.4.2. Unconfined Compressive Strength Test

Unconfined compressive strength testing was performed on cementitious material specimens at curing ages of 7, 14, and 28 days using a hydraulic servo-controlled testing machine. Throughout testing, the axial loading rate was maintained at 0.1 kN/s. The unconfined compressive strength was calculated based on the peak failure load. To mitigate experimental variability, three replicate specimens were tested for each mix group. The reported unconfined compressive strength value represents the arithmetic mean of these three measurements. In accordance with standard statistical outlier rejection criteria, if either the maximum or minimum value deviated from the mean by more than 15% of the median value, the outlier was excluded and the unconfined compressive strength was recalculated as the mean of the remaining two specimens. The entire dataset was discarded

if both extreme values exceeded this 15% deviation threshold. The test instrument is shown in Figure 3.



Figure 3. Pressure testing machine.

3. Results and Discussion

3.1. Analysis of Liquidity

The Figure 4 depicts the fluidity values of composite cementitious materials under alkali activation. All three alkali activators reduced fluidity; among them, Na_2SO_4 has the greatest effect on the flow value of the composite cementitious material, while NaOH and Na_2SiO_3 have the smallest effect. Among the tested formulations, mix W5 demonstrated the lowest fluidity at 258.5 mm, exceeding the lower threshold of the medium grade classification by 8.5 mm. Conversely, mix N4 achieved the highest fluidity at 385.4 mm, surpassing the minimum requirement for the good classification by 35.4 mm. Regarding engineering applications, conventional backfilling operations require materials meeting the medium fluidity standard, while confined workspaces necessitate good fluidity performance. Consequently, the alkali-activated composites universally satisfy the fluidity requirements for general backfilling applications.

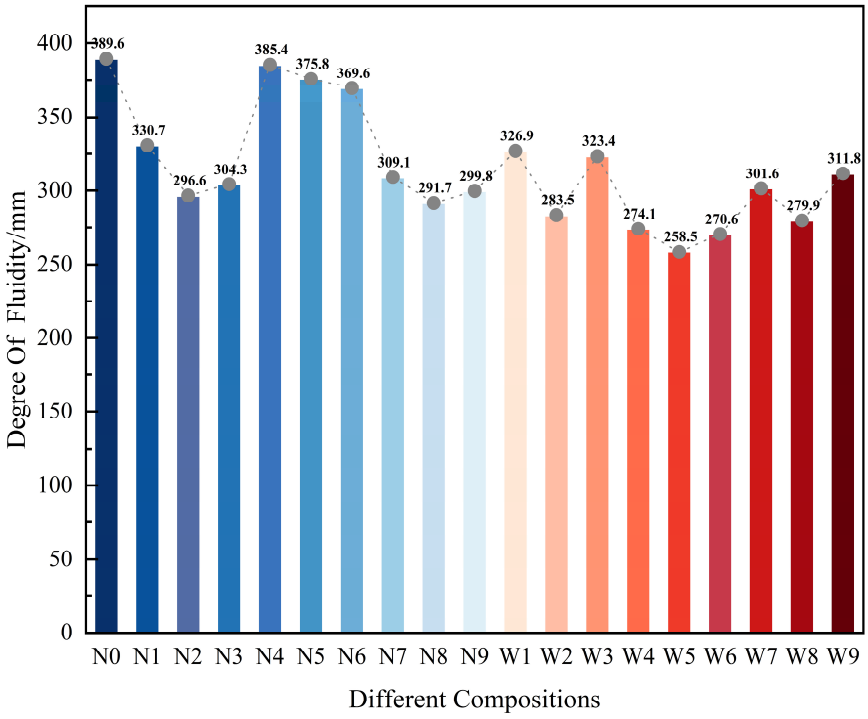


Figure 4. The fluidity value of composite cementitious materials under different orthogonal tests.

Figure 5 shows the fluidity value of the composite cementitious material under alkali excitation. As shown in the figure, the three alkali activators will reduce the flow value of the composite cementitious material. Among them, Na_2SO_4 has the greatest effect on the flow value of the composite cementitious material, while NaOH and Na_2SiO_3 have the smallest effect. This has a great influence on the liquidity value. Under different alkali excitations, the fluidity value of W5 was the lowest, being 258.5 mm, which is 8.5 mm higher than the lower limit of the 'general' grade in the fluidity grading standard. The fluidity value of N4 is the highest at 385.4 mm, which reaches the 'good' standard in the fluidity grading standard, and the lower limit of the 'good' grade in the fluidity grading standard is 35.4 mm higher. For the general backfilling project, it is necessary to ensure that the fluidity of the filling material is at the 'general' level. For the backfilling project of the narrow working surface, its fluidity must reach the 'good' standard.

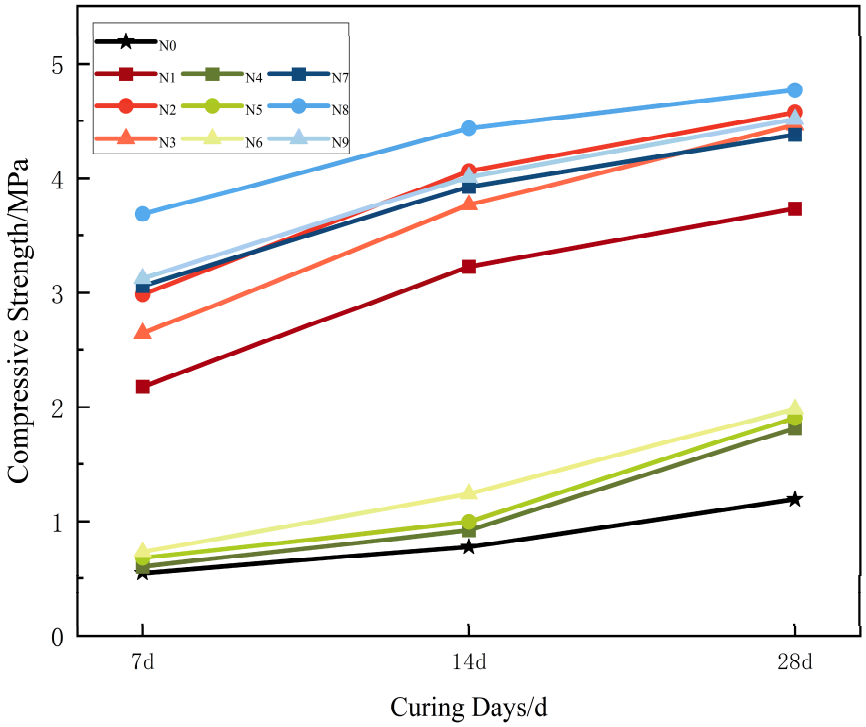


Figure 5. Effect of age on unconfined compressive strength of composite cementitious materials under single-alkali excitation.

3.2. Analysis of Unconfined Compressive Strength

3.2.1. Analysis of Key Factors Influencing Unconfined Compressive Strength Under Single-Activator Conditions

Table 5 shows the compressive strength of composite cementitious materials under single-alkali excitation. Compared with the group without alkali excitation, the compressive strength of composite cementitious materials is improved by three kinds of alkali activators, and the strength of composite cementitious materials is improved by Na_2SiO_3 and NaOH. The increase in Na_2SO_4 is greater than that in Na_2SiO_3. Among them, the compressive strength at 7 d, 14 d and 28 d under Na_2SiO_3 excitation was the largest, and the compressive strength at 7 d, 14 d and 28 d without alkali activator N0 increased by 573.49%, 470.05% and 299.25%, respectively. The 7 d, 14 d and 28 d compressive strength values of N2 under NaOH excitation ranked second, and the 7 d, 14 d and 28 d compressive strength of N0 without an alkali activator were increased by 2.439 MPa, 3.286 MPa and 3.379 MPa, respectively. Therefore, Na_2SiO_3 and NaOH were selected as alkali activators for subsequent mixed alkali excitation.

Table 5. Unconfined compressive strength of single alkali-activated composite cementitious material.

Specimens	Unconfined Compressive Strength/MPa		
	7 d	**14 d**	**28 d**
N0	0.547	0.778	1.194
N1	2.178	3.227	3.731
N2	2.986	4.064	4.573
N3	2.643	3.765	4.465
N4	0.603	0.925	1.813
N5	0.679	0.997	1.907
N6	0.734	1.241	1.982
N7	3.059	3.926	4.379
N8	3.684	4.435	4.767
N9	3.125	4.012	4.514

Figure 5 illustrates the influence of curing age on strength development under single-activator conditions. All systems exhibited progressive strength gain with increasing age. Specimens activated with Na_2SiO_3 or NaOH showed higher strength growth rates during the early 7-to-14 day period compared to the later 14-to-28 day phase. Conversely, Na_2SO_4 activated specimens demonstrated predominant strength development during mid-to-late stages, with comparatively modest overall enhancement. This performance divergence originates from distinct reaction mechanisms: strongly alkaline systems including Na_2SiO_3 and NaOH promote rapid polycondensation reactions enabling accelerated early strength development, though later-stage progression becomes diffusion-limited; whereas moderately alkaline Na_2SO_4 relies on gradual ettringite and calcium silicate hydrate formation, resulting in progressive strength evolution during extended curing.

3.2.2. Range Analysis and Analysis of Variance of Unconfined Compressive Strength Under Single-Activator Conditions

To investigate the effects of alkali activator type and dosage on the compressive strength of composite cementitious materials, range analysis and analysis of variance were employed. These methods facilitate the identification of primary influencing factors and enable determination of optimal parameter combinations through systematic comparison.

Range analysis is one of the commonly used analysis methods in orthogonal test data analysis. The calculation process of range analysis is relatively simple. By comparing the range values corresponding to the test results, the significance level of each factor to the target can be obtained. The range refers to the maximum difference between the test results of different levels of each factor. The calculation method is $k_{max} - k_{min}$. The larger the range, the higher the significance of the factor, and the greater the impact on the response target.

Analysis of variance (ANOVA) is a statistical method pioneered by British statistician F. A. Fisher. Variance analysis can determine the influence of each factor (independent variable) on the response target (dependent variable) by analyzing the influence of different independent variables on the response target. Compared with range analysis, variance analysis can take into account the influence of the fluctuation of a single factor on the overall experimental results, analyze the significance of the experimental results, and judge whether the fluctuation of the experimental data is due to a change in the factor level or experimental error. Therefore, variance analysis is often used in the analysis of orthogonal design results, and the results of range analysis are verified and supplemented.

Range analysis of unconfined compressive strength across curing ages under single-activator conditions is detailed in Table 6. The results demonstrate that the significance

ranking of factors affecting unconfined compressive strength follows: Alkali Activator Type (A) > Alkali Content (B). The range value for Factor A substantially exceeded that of Factor B, indicating that activator type is the dominant variable governing unconfined compressive strength development. Among the three activators, Na_2SiO_3 and NaOH exhibited significantly greater influence than Na_2SO_4. The optimal parameter combination derived from range analysis was A_3B_2.

The variance analysis of the compressive strength values of the composite cementitious materials at different ages under single alkali excitation is carried out, and the results are shown in Table 7. When the test index was 7d, 14d and 28d, the F test value of factor A was greater than the critical value of 99.0 when the confidence level was 99 %, which reached a highly significant level; when the test index is 7d and 14d, the F test value of factor B is greater than the critical value of 19.0 when the confidence is 95 %, reaching a significant level of influence. When the test index is 28d, the F test value of factor B is greater than the critical value of 9.0 when the confidence is 90 %, reaching an influential level. The order of the influence degree of each factor is A > B, and the significant influence law of each factor is generally consistent with the range analysis, which shows that the test results are reasonable.

Table 6. Range Analysis of Unconfined Compressive Strength Across Curing Ages with Different Single-Alkali Activators.

Range Value	Response Index	Alkali Activator Type (A)	Alkali Content (B)	Impact Order
7 d Unconfined Compressive Strength	k1	2.602	1.947	A > B
	k2	0.672	2.450	
	k3	3.289	2.167	
	R	2.617	0.503	
	Optimum Level	A_3	B_2	
14 d Unconfined Compressive Strength	k1	3.685	2.693	A > B
	k2	1.054	3.165	
	k3	4.124	3.006	
	R	3.070	0.473	
	Optimum Level	A_3	B_2	
28 d Unconfined Compressive Strength	k1	4.256	3.308	A > B
	k2	1.901	3.749	
	k3	4.553	3.654	
	R	2.653	0.441	
	Optimum Level	A_3	B_2	

Table 7. Analysis of Variance for Unconfined Compressive Strength (UCS) Across Curing Ages with Different Single-Alkali Activators.

Analysis of Variance	Factor	SS	DF	MF	F	P	Significance
7 d Unconfined Compressive Strength	A	11.049	2	5.524	581.376	0.002	***
	B	0.381	2	0.191	20.070	0.047	**
	Error	0.019	2	0.010	1		
14 d Unconfined Compressive Strength	A	16.540	2	8.270	967.880	0.001	***
	B	0.347	2	0.173	20.305	0.047	**
	Error	0.017	2	0.009	1		
28 d Unconfined Compressive Strength	A	12.674	2	6.337	419.296	0.002	***
	B	0.324	2	0.162	10.705	0.085	*
	Error	0.030	2	0.015	1		

Note: In order to distinguish the degree of significance, when F > F0.01 (f1, f2), it is said that the change of the factor level has a highly significant effect on the test results, which is recorded as ***; when F0.01 (f1, f2) > F > F0.05 (f1, f2), the change of the factor level has a significant effect on the test results, which is recorded as **; when F0.05 (f1, f2) > F > F0.10 (f1, f2), the change of the factor level has a certain influence on the test results, which is recorded as *, where F0.10 (f1, f2) = 9.0; f0.05 (f1, f2) = 19.0; f0.01 (f1, f2) = 99.0.

3.2.3. Analysis of Key Factors Governing Unconfined Compressive Strength Under Composite Activation

Table 8 shows the unconfined compressive strength of the composite cementitious material under the excitation of mixed alkali. Compared with the single-alkali excitation group, the compressive strength of the mixed-alkali excitation group is basically stronger than that of the single-alkali excitation group. When the modulus of water glass is 1.2 and the content of water glass is 8%, the unconfined compressive strength of the composite cementitious material is the largest, and the 28 d unconfined compressive strength reaches 7.653 MPa, which is 6.459 MPa higher than that of the 28 d unconfined compressive strength of the non-alkali excitation group.

Figure 6 is the influence of different moduli on the 28 d unconfined compressive strength of composite cementitious materials. From the diagram, it can be seen that the 28 d compressive strength increases first and then decreases with the increase in modulus. As the modulus increases, the content of NaOH decreases. The content of NaOH determines the alkalinity of the solution, and the high alkalinity promotes the dissolution of the aluminosilicate phase from the precursor particles. When the modulus is 1.4, the concentration of OH ions becomes smaller, the concentration of silicate ions provided by the water glass is too high, and the polymerization degree of silicate ions is large, which inhibits the formation of an enhanced gel phase and causes the strength to decrease. Conversely, when the modulus is too small to be 1.0, although the content of Na_2O is high, it is beneficial to the disintegration of the vitreous body, but the silicate ion concentration is lower and can only rely on Na_2O, so it is not conducive to the development of strength. NaOH promoted the disintegration of the composite cementitious material, and the silica gel in the water glass formed C-A-S-H gel with Ca^{2+} and Al^{3+}. Therefore, when the modulus is moderate, up to 1.2, the silicate concentration is appropriate while providing sufficient alkali, which promotes the formation of a stable silicon-aluminum gel network, and the structure is denser, so the compressive strength is greater.

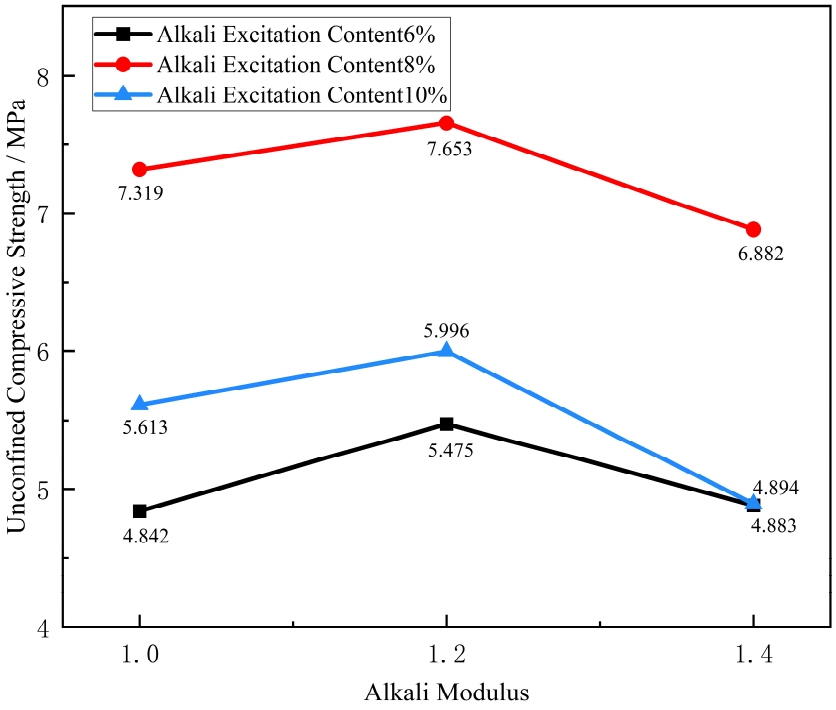


Figure 6. Effect of different moduli on 28 d unconfined compressive strength of composite cementitious materials.

Figure 7 shows the effect of different alkali content on the 28 d unconfined compressive strength of composite cementitious materials. It can be seen from the figure that the 28 d compressive strength also increases first and then decreases with the increase in alkali content. When the alkali content is 6%, the alkalinity is insufficient, the kaolinite in the coal gangue and the dicalcium silicate in the steel slag are not fully dissolved, the reaction is incomplete, and the strength is low. When the alkali content is 10%, the excessive OH concentration leads to the reaction being too fast, the local thermal stress increasing, and microcracks being generated; too much non-gelling sodium salt is produced, consuming effective alkali and increasing porosity; and the gel structure is loose due to rapid precipitation. Therefore, when the alkali content is 8%, it provides the best alkalinity, fully dissolves the Si/Al in the coal gangue and the Ca^{2+} in steel slag, and controls the reaction rate, which is conducive to orderly polycondensation to form a high-density gel, so the strength is greater.

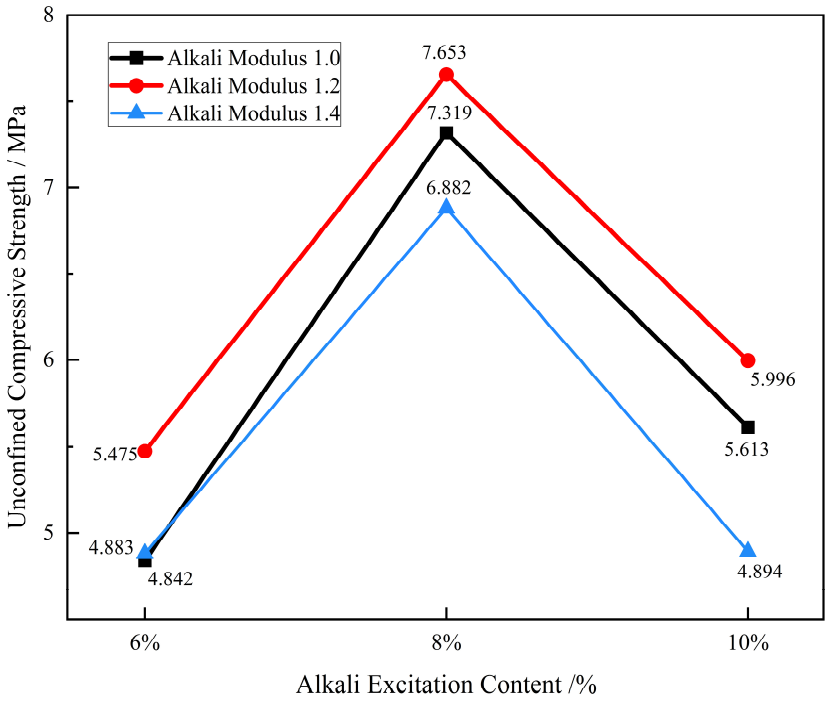


Figure 7. Effect of different alkali contents on 28 d unconfined compressive strength of cementitious materials.

Table 8. Unconfined compressive strength of alkali-activated composite cementitious materials.

Specimens	Unconfined Compressive Strength/MPa		
	7 d	14 d	28 d
W1	2.898	2.747	4.842
W2	3.673	4.171	5.475
W3	2.958	3.018	4.883
W4	5.438	5.177	7.319
W5	5.712	7.301	7.653
W6	5.049	5.231	6.882
W7	3.975	3.652	5.613
W8	4.196	4.523	5.996
W9	3.035	3.495	4.894

3.2.4. Range Analysis and Variance Analysis of Unconfined Compressive Strength Under the Condition of Composite Activator

The range analysis of the compressive strength values of the composite cementitious materials at different ages under the excitation of mixed alkali was carried out, and the

results are shown in Table 9. From the table, it can be seen that the primary and secondary order of the influence of each age factor on the compressive strength value under the compound alkali excitation is alkali modulus > alkali activator content, and when the alkali modulus is 1.2, the influence degree is the largest. According to the results of range analysis, the optimal ratio of the compressive strength of the composite cementitious materials under alkali excitation is A_2B_2.

The variance analysis of the compressive strength values of the composite cementitious materials at different ages under the excitation of mixed alkali was carried out, and the results are shown in Table 10. When the test index was 7 d and 28 d, the F test value of factor A was greater than the critical value of 99.0 when the confidence level was 99%, which reached a highly significant level of influence. The F test value of factor B is greater than the critical value of 19.0 when the confidence level is 95%, which reaches a significant influence level. When the test index was 14 d, the F test value of factor A was greater than the critical value of 99.0 when the confidence level was 99%, which reached a highly significant level of influence. The F test value of factor B is greater than the critical value of 9.0 when the confidence level is 90%, which reaches a significant level of influence. The influence degree of each factor is A > B, and the significant influence law of each factor is generally consistent with the range analysis, indicating that the test results are reasonable.

Table 9. Range analysis table of compressive strength of different alkali activators at different ages.

Range Value	Response Index	Alkali Modulus (A)	Alkali Content (B)	Impact Order
7 d Unconfined Compressive Strength	k1	3.176	4.104	A > B
	k2	5.340	4.527	
	k3	3.735	3.681	
	R	2.223	0.846	
	Optimum Level	A_2	B_2	
14 d Unconfined Compressive Strength	k1	4.237	5.183	A > B
	k2	6.653	5.691	
	k3	4.746	4.762	
	R	2.417	0.929	
	Optimum Level	A_2	B_2	
28 d Unconfined Compressive Strength	k1	5.067	5.925	A > B
	k2	7.285	6.375	
	k3	5.501	5.553	
	R	2.218	0.822	
	Optimum Level	A_2	B_2	

Table 10. Analysis of variance of compressive strength of different alkali activators at different ages.

Analysis of Variance	Factor	SS	DF	MF	F	P	Significance
7 d Unconfined Compressive Strength	A	8.026	2	4.013	144.170	0.007	***
	B	1.074	2	0.537	19.300	0.049	**
	Error	0.056	2	0.028	1		
14 d Unconfined Compressive Strength	A	9.738	2	4.869	140.076	0.007	***
	B	1.298	2	0.649	18.677	0.051	*
	Error	0.070	2	0.035	1		
28 d Unconfined Compressive Strength	A	8.210	2	4.105	213.558	0.005	***
	B	0.991	2	0.495	25.767	0.037	**
	Error	0.038	2	0.019	1		

Note: In order to distinguish the degree of significance, when F > F0.01 (f1, f2), it is said that the change of the factor level has a highly significant effect on the test results, which is recorded as ***; when F0.01 (f1, f2) > F > F0.05 (f1, f2), the change of the factor level has a significant effect on the test results, which is recorded as **; when F0.05 (f1, f2) > F > F0.10 (f1, f2), the change of the factor level has a certain influence on the test results, which is recorded as *, where F0.10 (f1, f2) = 9.0; f0.05 (f1, f2) = 19.0; f0.01 (f1, f2) = 99.0.

3.3. Optimization Design of Orthogonal Test Scheme Under Complex Alkali Excitation

In order to comprehensively consider the compressive strength and fluidity of cementitious materials under the excitation of mixed alkali, it is necessary to use the efficiency coefficient method to determine the optimal ratio of cementitious material strength. The efficacy coefficient method is a mathematical method for comprehensive analysis of one or more indicators based on the principle of multi-objective programming. In this study, the compressive strength and fluidity of 7 d and 28 d under the excitation of mixed alkali were used as the evaluation indexes d1, d2 and d3. The comprehensive influence of these three evaluation indexes was reflected by the efficacy coefficient method, and then the optimum ratio of cementitious materials under the excitation of mixed alkali was determined.

The efficacy coefficient method stipulates that the efficacy coefficient of the index with the highest assessment value is 1, and the efficacy coefficient of the remaining indicators is the ratio of the assessment index value to the highest index value. The calculation method of the total efficacy coefficient D is that the value of $D = \sqrt[3]{d_1 d_2 d_3}$ reflects the overall situation of the assessment index. The larger the D value, the better the scheme. Then, by calculating the arithmetic mean value Ki of the D value of different factors at a certain level, the optimal mix ratio of the filling material is determined.

Table 11 is the calculation table of the efficiency coefficient of the orthogonal test of cementitious materials under the excitation of mixed alkali. According to the analysis in the table, considering the compressive strength and fluidity of the composite cementitious material at 7 d and 28 d under the excitation of compound alkali, the total efficiency coefficient of the cementitious material is the highest (D = 0.924) in the scheme W5 group, that is, when the modulus of the water glass is 1.2 and the content of the water glass is 8%.

Table 11. Calculation table of efficiency coefficient of orthogonal test under compound alkali excitation.

Specimens	Efficiency Coefficient			Overall Efficacy Coefficient
	d_1	d_2	d_3	$D=\sqrt[3]{d_1 d_2 d_3}$
W1	0.507	0.633	1	0.685
W2	0.643	0.715	0.867	0.736
W3	0.518	0.638	0.989	0.689
W4	0.952	0.956	0.838	0.914
W5	1	1	0.790	0.924
W6	0.884	0.899	0.829	0.870
W7	0.696	0.733	0.920	0.778
W8	0.735	0.783	0.856	0.790
W9	0.531	0.639	0.954	0.687

4. Study on Microstructure Characteristics

4.1. XRD Analysis

Figure 8 is the XRD pattern of composite cementitious materials with different modulus under alkali excitation. From the X-ray diffraction test results of composite cementitious materials, it can be seen that the main crystal phases of composite cementitious materials include dicalcium silicate ($2CaO{\cdot}SiO_2$, C_2S), tricalcium silicate ($3CaO{\cdot}SiO_2$, C_3S), Ca $(OH)_2$, $CaCO_3$ and some quartz (SiO_2) that did not participate in the reaction, which provided a large number of ion components for the hydration reaction of the composite cementitious materials and promoted the hydration reaction of the inorganic cementitious materials.

The intensity change in the quartz (SiO_2) diffraction peak was observed, and it was found that it decreased first and then increased with the increase in the modulus of the activator. When the modulus is low, the alkalinity of the system is high, the concentration of OH^- is high, and the intensity of the quartz peak decreases. However, when the modulus

is too low, excessive OH^- will lead to the rapid formation of a dense hydration product layer on the mineral surface, hindering the continuous dissolution of the internal quartz. At the same time, the rapidly generated gel may encapsulate the unreacted particles, but inhibit the later reaction, which explains the low strength of the low modulus sample. With the increase in modulus, the concentration of OH^- decreases, but the polymerization ability of silicate increases. The dissolution rate of quartz and the formation rate of hydration products reach equilibrium, and the gel structure is more uniform. Therefore, the strength of the quartz peak decreases and the area of the dispersion peak increases. When the modulus is too high, the alkalinity is insufficient, the quartz dissolution is inhibited, the residual quartz increases, and the diffraction peak intensity rebounds.

In summary, the modulus of the alkali activator significantly affects the dissolution rate of quartz and the formation of the C-S-H/C-A-S-H gel by regulating the concentration of OH^- and silicate species, and then determines the mechanical properties of composite cementitious materials. Properly increasing the modulus is conducive to the formation of more gels, but a too high or too low modulus is not conducive to the full hydration reaction of the system.

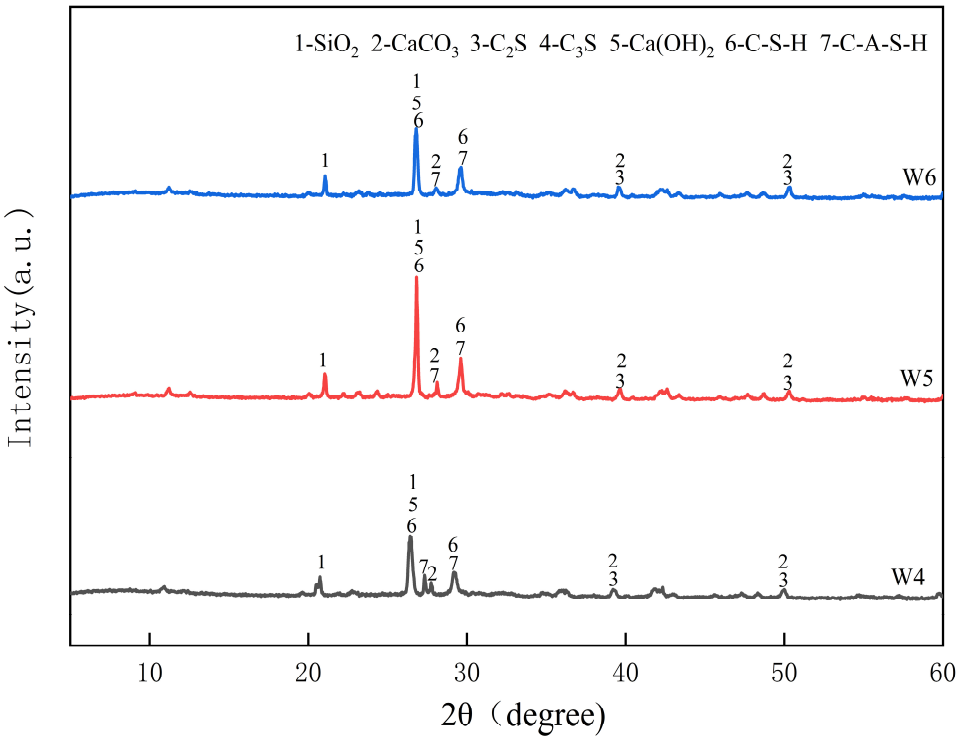
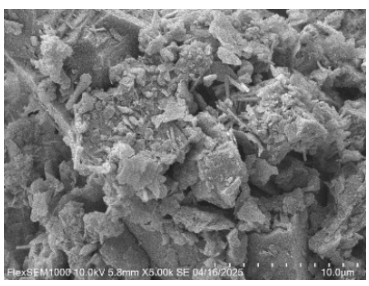


Figure 8. XRD patterns of composite cementitious materials with different modulus.

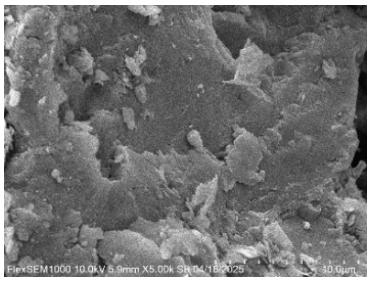
4.2. SEM Analysis

In order to further explore the internal reaction mechanism and the source of strength system of composite cementitious materials, the sample fragments of composite cementitious materials with different moduli under alkali excitation were selected for a scanning electron microscope test, as shown in Figure 9. When the modulus is 1.0, only a small amount of C-S-H and C-A-S-H gels are formed in the system, which mainly exist in a small amount of needle-like crystals and flocculent forms, interlaced with each other and closely filled between the particle voids, but there are many voids and the structure is loose. When the modulus is increased to 1.2, the hydration products in the system increase; in addition to the formation of needle-like products, a large number of amorphous gel-phase substances are also generated. Combined with the XRD results, it is inferred that this is

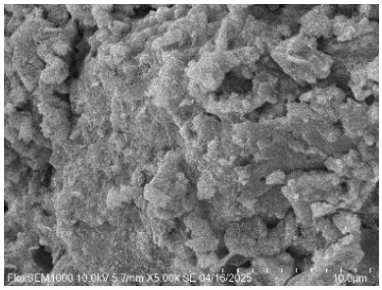
C-S-H gelling and C-A-S-H gelling. The dense matrix formed greatly optimizes the contact form of the microstructure of the material, making the structure of the sample smoother and tighter. In addition, agglomerated C-S-H gel, C-A-S-H gel and layered Ca (OH) 2 grow in large quantities on the surface and voids of the material, making the microstructure of the material denser, thus forming a more stable network structure. When the modulus reaches 1.4, due to the decrease in NaOH content in the alkali activator, the decomposition of the precursor of the composite cementitious material is limited, resulting in a gradual decrease in the generated gel material; the densification degree of the microstructure is reduced and the generated gel cannot fill the gap between the particles, thus the strength is reduced.



(**a**) W4 SEM scan photos



(**b**) W5 SEM scan photos



(**c**) W6 SEM scan photos

Figure 9. SEM images of composite cementitious materials with different modulus.

5. Conclusions

The fluidity, unconfined compressive strength and microscopic mechanism of composite cementitious materials were studied by different alkali activators and different moduli and contents.

(1) The three alkali activators will reduce the fluidity value of the composite cementitious material. Among them, Na_2SO_4 has the least influence on the fluidity value of the composite cementitious material, while NaOH and Na_2SiO_3 have a greater influence on the fluidity value. However, the fluidity values of the composite cementitious material under the excitation of the three alkali activators can meet the requirements of the general backfill project.

(2) Under the single-doped alkali excitation, the three alkali-activated materials all improved the compressive strength of the composite cementitious material, and the strength influence of the Na_2SiO_3 and NaOH cementitious materials was greater than that of Na_2SO_4. Through the range analysis and variance analysis, it can be seen that the primary and secondary order of the influence on the compressive strength value under the single-doped alkali excitation is alkali activator > alkali activator content, and the optimal ratio of the compressive strength value of the composite cementitious material under the single-doped alkali excitation is A_3B_2.

(3) The unconfined compressive strength of composite cementitious materials under alkali excitation is basically stronger than that of the single-alkali excitation group, and increases first and then decreases with the increase in modulus and alkali content. When the modulus is 1.2 and the content is 8%, the unconfined compressive strength reaches its maximum at 28 d; this being 7.653 MPa, which is 540.95% and 299.25% higher than that of the non-alkali excitation group and the single-alkali excitation group. Through range analysis and variance analysis, it can be seen that the primary and secondary order of the influence of each age factor on the compressive strength value under compound alkali excitation is alkali modulus > alkali activator content,

and the optimal ratio of the compressive strength value of the composite cementitious material under the compound alkali excitation is A_2B_2.

(4) Considering the compressive strength and fluidity of composite cementitious materials at 7 d and 28 d, and through the calculation table of efficiency coefficient, it is known that the total efficiency coefficient of cementitious materials is the highest (D = 0.924) when the scheme W5 group and the scheme W5 group are selected, that is, when the modulus of water glass is 1.2 and the content of water glass is 8%.

(5) By comparing the XRD and SEM images of different moduli of composite cementitious materials under alkali excitation, it can be seen that the strength of composite cementitious materials under alkali excitation is mainly established by the fracture of Si-O and Al-O bonds, and the cementation between C-S-H gel and C-A-S-H gel and particles generated by hydration reaction.

Author Contributions: Conceptualization, X.Z. and M.Z.; methodology, X.Z. and Y.M.; software, H.L.; validation, X.Z. and M.Z.; formal analysis, H.L.; investigation, X.Z.; resources, Y.M.; data curation, Y.M.; writing—original draft preparation, X.Z.; writing—review and editing, M.Z.; visualization, H.L.; supervision, Y.M.; project administration, X.Z.; funding acquisition, Y.M. All authors have read and agreed to the published version of the manuscript.

Funding: This research received no external funding.

Data Availability Statement: The original data supporting the conclusion of this paper will be provided by the authors as needed.

Conflicts of Interest: Authors Xuejing Zhang and Mingyuan Zhou were employed by the company Shaanxi Building Materials Technology Group Co., Ltd. The remaining authors declare that the research was conducted in the absence of any commercial or financial relationships that could be construed as a potential conflict of interest.

References

1. Lu, Z.; Tan, Q.; Lin, G.; Wang, D. Properties investigation of recycled aggregates and concrete modified by accelerated carbonation through increased temperature. *Constr. Build. Mater.* **2022**, *341*, 127813. [CrossRef]
2. Wang, Z.F.; Pan, C.; Jiang, Y.; Zhong, J.; Zhu, J. Efficient separation of coarse aggregates and cement mortar in the recycled concrete by water jet demolition. *Mater. Lett.* **2023**, *333*, 133623. [CrossRef]
3. Tošić, N.; Martínez, D.; Hafez, H.; Reynvart, I.; Ahmad, M.; Liu, G.; Fuente, A. Multi-recycling of polypropylene fibre reinforced concrete: Influence of recycled aggregate properties on new concrete. *Constr. Build. Mater.* **2022**, *346*, 128458. [CrossRef]
4. Wang, W.C.; Wang, P.; Wu, Z.; Li, Y.; Yang, S. Study on the air permeability characteristics of coal gangue dump slope gangue particles. *Coal Sci. Technol.* **2024**, *52*, 139–151.
5. Zhang, C. *Technology of Coal Gangue Resource Recycling and Utilization*; Chemical Industry Press: Beijing, China, 2017.
6. Zhao, X.; Wang, L.; Xu, Y.; Ni, J.M. Economic benefit analysis of coal gangue calcination and grinding process. *Sci. Technol. Innov. Her.* **2022**, *19*, 28–31.
7. Fang, S.; Lam, E.; Li, B.; Wu, B. Effect of alkali contents, moduli and curing time on engineering properties of alkali activated slag. *Constr. Build. Mater.* **2020**, *249*, 118799. [CrossRef]
8. Chen, X.Q.; Wang, G.T.; Dong, Q.; Zhao, X.; Wang, Y. Microscopic characterizations of pervious concrete using recycled Steel Slag Aggregate. *J. Clean. Prod.* **2020**, *254*, 120149. [CrossRef]
9. Fang, Y.; Su, W.; Zhang, Y.; Zhang, M.; Ding, X.; Wang, Q. Effect of accelerated precarbonation on hydration activity and volume stability of steel slag as a supplementary cementitious material. *Therm. Anal. Calorim.* **2022**, *147*, 6181–6191. [CrossRef]
10. Bogas, J.; Real, S.; Carriço, A.; Abrantes, J.; Guedes, M. Hydration and phase development of recycled cement. *Cem. Concr. Compos.* **2022**, *127*, 1105–1112. [CrossRef]
11. Ding, R.; Li, H.; Tian, H.; Wang, H.; Chen, Y.; Li, W. Influence of Steel Slag Content on the Characteristics of "One-step" Alkali-activated Composite Cementitious Materials. *J. Wuhan Univ. Technol. Mater. Sci. Ed.* **2025**, *40*, 104405. [CrossRef]
12. Liao, Z.; Xue, W.; Liao, L.; Hao, R.; Shen, L.; Cui, D. A Study on the Effect of Different Cementitious Materials on the Mechanical Properties and Microscopic Characteristics of Alkali-Activated Green Ultra-High Performance Concrete (GUHPC). *Materials* **2025**, *18*, 2163. [CrossRef]

13. Liu, Y.; He, B.; Chen, Z.; Jing, X.; Cang, D.; Zheng, Y.; Zhang, L. Contribution of calcium-containing minerals on the mechanical properties of alkali-activated materials: A study of carbonation steel slag. *Constr. Build. Mater.* **2025**, *18*, 2163. [CrossRef]
14. Su, P.; Xia, M.; Chen, K.; Wang, H.; Li, X.; Zhou, Z.; Zhang, R.; Zhang, L.; Zhao, S. Study on the Solidification/Stabilization of MSWI Fly Ash by Composite Alkali-Activated Cementitious Materials. *ACS Omega* **2025**, *10*, 5659–5667. [CrossRef] [PubMed]
15. Duan, Z.; Zhao, W.; Ye, T.; Xiao, J. Performance optimization and environmental assessment of novel alkali-activated binders containing carbonated recycled concrete powder. *J. Clean. Prod.* **2024**, *25*, 144145. [CrossRef]
16. Lou, B.; Vrålstad, T. Strength Development of Metakaolin-Based Alkali-Activated Cement. *Appl. Sci.* **2023**, *13*, 13062. [CrossRef]
17. Feng, D.; Wang, J.; Wang, Y.; Xiao, X.; Hou, W.; Liang, S. Alkali-activated geopolymer materials prepared from coal gangue and municipal solid waste incineration byproducts. *J. Build. Eng.* **2023**, *80*, 108074. [CrossRef]
18. Yu, Z.; Wang, B.; Li, T.; Wang, W. Toughness study of polyacrylamide-modified slag/fly ash-based alkali-activated cementitious materials. *Constr. Build. Mater.* **2024**, *450*, 138622. [CrossRef]
19. Yang, Z.; Tang, W.; Zhang, D.; Zang, J.; Wang, K.; Zhao, Z. Hydration mechanism of alkali-activated cementitious materials entirely prepared by solid wastes. *J. Build. Eng.* **2024**, *97*, 110921. [CrossRef]
20. Zhang, W.; Yu, H.; Yin, B.; Akbar, A.; Dai, J.G.; Zhang, X.; Liew, K.M. Effects of recycled carbon fibers on mechanical and piezoresistive properties and environmental impact in alkali-activated cementitious materials. *J. Clean. Prod.* **2024**, *450*, 141902. [CrossRef]
21. Sun, J.; Hou, S.; Guo, Y.; He, W.; Cui, Y.; Zhang, P. Effects of high-temperature curing on hydration and microstructure of alkali-activated typical steel slag cementitious material. *Dev. Built. Environ.* **2024**, *17*, 100314. [CrossRef]
22. Wang, F.; Gu, X.; Wang, Q.; Liu, J.; Xu, X.; Zhao, Y. Utilization of Copper–Molybdenum Tailings to Enhance the Compressive Strength of Alkali-Activated Slag-Fly Ash System. *Buildings* **2024**, *14*, 1031. [CrossRef]
23. Goufi, N.; Kaid, N.; Kerdal, D.E.D.; Idir, R. Sustainable cementitious materials: Exploring alkali-activated binders. *Proc. Inst. Civ. Eng. Constr. Mater.* **2023**, *177*, 233–248. [CrossRef]
24. Cui, P.; Wan, Y.; Shao, X.; Ling, X.; Zhao, L.; Gong, Y.; Zhu, C. Study on Shrinkage in Alkali-Activated Slag–Fly Ash Cementitious Materials. *Materials* **2023**, *16*, 3958. [CrossRef] [PubMed]
25. Liu, B.; Geng, S.; Ye, J.; Liu, X.; Lin, W.; Wu, S.; Qian, K. A preliminary study on waste marble powder-based alkali-activated binders. *Constr. Build. Mater.* **2023**, *378*, 131094. [CrossRef]
26. Palmero, P.; Formia, A.; Tulliani, J.M.; Antonaci, P. Valorisation of Alumino-Silicate Stone Muds: From Wastes to Source Materials for Innovative Alkali-activated Material. *Cem. Concr. Compos.* **2017**, *83*, 251–262. [CrossRef]
27. Yu, X.; Shi, J.; He, Z.; Ling, X.; Yalçınkaya, Ç.; Cuesta, V.R.; Gencel, O. Review of the materials composition and performance evolution of green alkali-activated cementitious materials. *Clean. Technol. Environ. Policy* **2023**, *25*, 1439–1459. [CrossRef]
28. Granizo, M.L.; Alonso, S.; Blanco-Varela, M.T.; Palomo, A. Alkaline Activation of Metakaolin: Effect of Calcium Hydroxide in the Products of Reaction. *J. Am. Ceram. Soc.* **2002**, *53*, 225–231. [CrossRef]
29. Zhang, S.; Wang, C.; Gao, G. Study of the Mechanical Properties of Alkali-Activated Solid Waste Cementitious Materials at the Interface. *ACS Omega* **2022**, *19*, 26531–26536. [CrossRef]
30. Song, Q.; Guo, M.Z.; Ling, T.C. A review of elevated-temperature properties of alternative binders: Supplementary cementitious materials and alkali-activated materials. *Constr. Build. Mater.* **2022**, *341*, 127894. [CrossRef]
31. Elahi, A.M.M.; Hossain, M.M.; Karim, M.R.; Zain, M.F.M.; Shearer, C. A review on alkali-activated binders: Materials composition and fresh properties of concrete. *Constr. Build. Mater.* **2020**, *260*, 119788. [CrossRef]
32. Zhang, Q.; Ji, T.; Yang, Z.X.; Wang, C.Q.; Wu, H. Influence of different activators on microstructure and strength of alkali-activated nickel slag cementitious materials. *Constr. Build. Mater.* **2020**, *235*, 117449. [CrossRef]
33. Yang, Y.; Yu, S.; Hu, A.; Cao, Y.; Bai, Y. Mechanical properties and damage model of alkali activated polymer solidified soil containing coal gangue powder. *Sci. Rep.* **2025**, *15*, 18666. [CrossRef]
34. Lazorenko, G.; Kasprzhitskii, A.; Yatsenko, E.; Li, W.E.; Chaudhary, S. Towards coal mining waste valorization: Gangue as resource for the production of geopolymer and related alkali-activated materials. *Green Technol. Sustain.* **2025**, *3*, 100205. [CrossRef]
35. Zhang, L.; Zhang, S.; Wang, Q.; Zhang, W.; Li, Z. Sustainable alkali-activated materials: Leveraging spontaneous combustion coal gangue for enhanced cementitious performance. *Mater. Today Commun.* **2024**, *41*, 111044. [CrossRef]
36. Wang, X.; Liu, F.; Li, L.; Chen, W.; Cong, X.; Yu, T.; Zhang, B. Study on the Compressive Strength and Reaction Mechanism of Alkali-Activated Geopolymer Materials Using Coal Gangue and Ground Granulated Blast Furnace Slag. *Materials* **2024**, *17*, 3659. [CrossRef] [PubMed]
37. Wang, X.; Liu, F.; Pan, Z.; Chen, W.; Muhammad, F.; Zhang, B.; Li, L. Geopolymerization of Coal Gangue via Alkali-Activation: Dependence of Mechanical Properties on Alkali Activators. *Buildings* **2024**, *14*, 787. [CrossRef]
38. Liu, C.; Wang, C.; Wu, J.; Gao, M. Calcined Coal Gangue Fines as the Substitute for Slag in the Production of Alkali-Activated Cements and Its Mechanism. *Processes* **2022**, *10*, 1557. [CrossRef]
39. Wang, C.; Liu, C.; Zhang, L.; Wang, C.; Xu, S.; Yang, J. Exploring calcined coal gangue fines as the total substitute of fly ash in the production of alkali-activated slag/fly ash materials. *Case Stud. Constr. Mater.* **2022**, *17*, e01332. [CrossRef]

40. Zang, B.; Yan, B.; Li, Y. Study on mechanical properties, freeze–thaw and chlorides penetration resistance of alkali activated granulated blast furnace slag-coal gangue concrete and its mechanism. *Constr. Build. Mater.* **2023**, *366*, 130218. [CrossRef]
41. Ma, H.; Chen, H.; Zhu, H.; Shi, Y.; Ni, Y.; Huo, Q.; Hang, Z. Study on the drying shrinkage of alkali activated coal gangue-slag mortar and its mechanisms. *Constr. Build. Mater.* **2019**, *225*, 204–213. [CrossRef]
42. Han, R.; Guo, X.; Guan, J.; Yao, X.; Hao, Y. Activation Mechanism of Coal Gangue and Its Impact on the Properties of Geopolymers: A Review. *Polymers* **2022**, *14*, 3861. [CrossRef]
43. Chen, Y.; Ma, H.; Zhu, H.; Li, W.; Xin, M.; Liu, Y.; Guo, Y. Study on chloride binding capability of coal gangue based cementitious materials. *Constr. Build. Mater.* **2018**, *167*, 649–656. [CrossRef]
44. Wang, Q.; Cheng, Z.; Zhou, F.; Cai, J.; Yuan, L.; Feng, X.; Wang, L.; Zhang, J.; Li, X. Response Surface Optimization of Coal-Based Geopolymer Grouts for Enhanced Anti-Dispersion Performance. *J. Build. Eng.* **2026**, *117*, 114882. [CrossRef]
45. Ma, L.; Zhang, X.; Liu, F.; Liu, Z.; Li, F. Strength Characteristics and Mechanism of Red Mud-Fly Ash Stabilized Coal Gangue Base. *J. Build. Mater.* **2023**, *26*, 762–770.
46. Duan, S.; Liao, H.; Cheng, F.; Song, H.; Yang, H. Investigation into the synergistic effects in hydrated gelling systems containing fly ash, desulfurization gypsum and steel slag. *Constr. Build. Mater.* **2018**, *187*, 1113–1120. [CrossRef]
47. Sadique, M.; Al Nageim, H.; Atherton, W.; Seton, L.; Dempster, N. A new composite cementitious material for construction. *Constr. Build. Mater.* **2012**, *35*, 846–855. [CrossRef]
48. Wang, M.; Xu, J.; Li, T.; Liu, H.; Qu, L. Comprehensive Performance Evaluation of Steel Slag–Slag–Desulfurization Gypsum Ternary Solid Waste Cementitious Material Based on Principal Component Analysis. *Buildings* **2025**, *15*, 645. [CrossRef]
49. Ge, Y.; Liu, X.; Shui, Z.; Gao, X.; Zheng, W.; Zhu, Z.; Zhao, X. Design and Preparation Technology of Green Multiple Solid Waste Cementitious Materials. *Materials* **2024**, *17*, 1998. [CrossRef] [PubMed]

Disclaimer/Publisher's Note: The statements, opinions and data contained in all publications are solely those of the individual author(s) and contributor(s) and not of MDPI and/or the editor(s). MDPI and/or the editor(s) disclaim responsibility for any injury to people or property resulting from any ideas, methods, instructions or products referred to in the content.